ADVANCED FUNCTIONAL MATERIALS
www.afm-journal.de

www.MaterialsViews.com

Achieving Outstanding Mechanical Performance in Reinforced Elastomeric Composite Fibers Using Large Sheets of Graphene Oxide

Mohammad Ziabari Seyedin, Joselito M. Razal, Peter C. Innis, Rouhollah Jalili, and Gordon G. Wallace**

A simple fiber spinning method used to fabricate elastomeric composite fibers with outstanding mechanical performance is demonstrated. By taking advantage of the large size of as-prepared graphene oxide sheets (in the order of tens of micrometers) and their liquid crystalline behavior, elastomeric composite fibers with outstanding low strain properties have been fabricated without compromising their high strain properties. For example, the modulus and yield stress of the parent elastomer improved by 80- and 40-fold, respectively, while maintaining the high extensibility of ~400% strain inherent to the parent elastomer. This outstanding mechanical performance was shown to be dependent upon the GO sheet size. Insights into how both the GO sheet size dimension and dispersion parameters influence the mechanical behavior at various applied strains are discussed.

1. Introduction

High performance elastomeric composites are those that have outstanding low strain properties (i.e., high stiffness and high yield stress) and high strain properties (i.e., uncompromised/sustained extensibility).[1–3] Imparting high stiffness and yield stress in soft elastomeric polymers is typically achieved using inherently stiff reinforcing fillers like clays,[1,4,5] nanotubes,[2,6–10] and graphene[3,11–15] (to name a few). In most cases, when these fillers are used, a decrease in extensibility is observed when stiffness and yield stress are increased, compromising the overall performance.[2,3,6,7,11,14]

The stiffness and extensibility of an elastomer originates from the unique phase segregation of the two distinct components – the ordered domains of hard segments and the entangled chains of soft segments.[16–19] In stiffened elastomeric composites, poor extensibility results from the non-selective reinforcement of both hard and soft segments. In such a case, while the inherent rigidity of the filler translates to the stiffness of the hard and the soft segments, it impedes the extensibility of the soft segment phase. Achieving preferential reinforcement within hard segment domains would prevent steric hindrance during soft segment chain extension and potentially allow extensibilities as high as that of the parent (unfilled) elastomer.[1,2] The preferential reinforcement of hard segment domains within elastomeric composite fibers has yet to be realized. The development of high performance elastomeric composite fibers is critical for a variety of applications including sports apparels, automotive, and aerospace.[16,20,21] Previous reports on elastomeric composites (in the form of films) that demonstrate improved performance have employed clay[1] and single walled carbon nanotube (SWCNT)[2] as fillers, employing solvent exchange[1] or SWCNT functionalization[2] as the methods to induce preferential reinforcement. In this report, graphene oxide (GO) sheets of varying sizes have been evaluated as reinforcing fillers, and the composite solutions from which the fibers are obtained (referred to as "spinning formulations") are prepared by a simple solution mixing. We propose that the use of large GO sheets (that spontaneously form an LC phase at the concentration used) can induce compatibility with the hard segment domains of the PU elastomer without interrupting its soft segment phase. This work demonstrates the importance of GO sheet size in determining selective interaction between the LCGO domains and the hard segment domains to achieve optimal performance. This was experimentally achieved by modulating the LC behavior in the LCGO dispersions used via the progressive reduction of GO sheet size. The observed decrease in performance with GO sheet size is corroborated with the analysis of the proposed model on how sheet size influences the modulus and elastic recovery of the elastomeric fibers produced here. This work not only demonstrates a new and highly scalable method in fabricating high performance elastomeric fibers, it also provides the understanding of the origin of high stiffness and high extensibilities when LCGO is used as filler.

M. Z. Seyedin, Prof. J. M. Razal, Prof. P. C. Innis, Dr. R. Jalili, Prof. G. G. Wallace
Intelligent Polymer Research Institute
ARC Centre of Excellence for Electromaterials Science
AIIM Facility, Innovation Campus
University of Wollongong
Wollongong, NSW 2522, Australia
E-mail: joselito.razal@deakin.edu.au; gwallace@uow.edu.au
M. Z. Seyedin, Prof. J. M. Razal
Institute for Frontier Materials
Deakin University
Geelong, VIC 3216, Australia

DOI: 10.1002/adfm.201402167

The recent progress in the synthesis and processing of LCGO dispersions that contain large sheets have enabled fabrication of various GO architectures in a range of forms (i.e., fibers, films, and printed assemblies) and the potential for scalability.[22–27] Due to the demonstrated versatility of LCGO, which can be produced in a range of organic solvents,[28] new opportunities for polymer nanocomposites that benefit from the outstanding properties of the inherently large GO sheets may be realized. LCGO has been used recently to produce polymer composite fibers by in situ polymerization techniques and achieved enhanced mechanical properties.[29,30] To date, however, little is known about how the GO sheet size influences the processability, how the LC behavior inherent to GO dispersions will be affected when a polymer component is added, and ultimately, how the combined effect of sheet size and the resultant liquid crystallinity will affect the mechanical properties of the composite fibers. Here we address these important points by developing polymer composite formulations suitable for fiber production via a wet-spinning process. Fibers have been produced from a medical grade polyurethane (PU), as the elastomer matrix, and compared to three significantly different GO sheet sizes as the reinforcing filler. It was postulated that the addition of GO would significantly enhance the mechanical properties of the parent elastomer and such properties would vary with the GO sheet size.

2. Results and Discussions

2.1. GO Sheet Size, Liquid Crystallinity and Spinnability

GO dispersions that contain GO sheets of varying size and size polydispersity were prepared following previously reported methods to form DMF-based liquid crystalline GO dispersions.[28] The as-prepared GO dispersion contained sheets as large as 38.8 μm with a mean lateral size of 12.1 μm and a size polydispersity (SPD, see Supporting Information for calculation) of 0.67. This parent GO dispersion is herein referred to as LGO (large graphene oxide, **Table 1**). GO dispersions with smaller sheets were prepared by deliberately breaking up the LGO sheets using two different sonication conditions. For instance, GO dispersions with medium GO sheets (MGO) were obtained following a low power 10 minute bath sonication of the LGO dispersions, while small GO sheets (SGO) were obtained by using a high power 30 minute probe sonication of the LGO dispersion. The maximum sheet size found in MGO and SGO dispersions were 15.7 μm and 1.2 μm, respectively. The mean GO sheet size and polydispersity were also significantly different from each other. MGO had a mean sheet size of 2.5 μm and an SPD of 0.96, while SGO had a mean sheet size and an SPD of 0.3 μm and 0.57, respectively. Representative SEM images for each dispersion are shown in **Figure 1**a-c.

These three dispersions displayed different liquid crystalline (LC) behavior (Figure 1d-e). At 1.5 mg ml^{-1} GO concentration for example, the LGO dispersion displayed birefringence under the cross polarizer typical for LC solutions with fully nematic phase. The MGO dispersion, on the other hand, displayed relatively weak birefringence (than LGO) typical of biphasic LC behavior. The SGO dispersion did not display any birefringence implying that the GO dispersion only contained isotropic phase.

All PU/GO spinning formulations were prepared to contain 1.5 mg ml^{-1} GO and 50 mg ml^{-1} PU. The PU and GO concentrations were kept the same for all samples to ensure that all PU/GO fibers have the same PU and GO content. This formulation corresponded to 2.9 wt.% of GO (equivalent to a volume fraction, ϕ of 0.016) in the final PU/GO fiber composition (see Supporting Information for detailed calculations). Interestingly, all PU/GO spinning formulations displayed birefringence similar to their parent GO dispersions (Figure 1g-i), with only the PU/LGO exhibiting fully nematic phase that has ordered domains similar to the pure LGO dispersion. Importantly, despite the high viscosity of the resulting formulations, due to the addition of high PU concentration, the LC characteristics of anisotropic LGO domains were similar in nature. This retained LC behavior of LGO after the addition of PU indicates the very high compatibility of PU and GO.

A non-solvent based wet-spinning method, described in previous reports,[24,31–35] was employed to prepare fibers from PU and PU/GO formulations. Using isopropanol as the non-solvent bath, all formulations were readily spinnable whereby continuous fibers exceeding 100 meters were successfully spun and collected onto a spool (**Figure 2**a). Due to the differences in the coagulation rate of each spinning formulations, their cross-sectional shapes differed (Figure 2b, **800**×).[35–38] The pure PU fiber appeared flat (due to the fast coagulation rate) while the PU/GO composite fibers were more rounded (due to the slow coagulation rate), albeit not perfectly circular. The lower coagulation rate of the PU/GO formulations is due to the addition of the amphiphilic GO which decreases the mass transfer rate difference between the solvent (DMF) of the spinning formulation and the non-solvent (isopropanol) coagulation bath. The typical fiber diameters (equivalent to an area of a circle) are between 65 to 75 μm. The observed ordered structures in PU/LGO dispersion are resonated in the cross-sectional morphology of its fiber suggesting that LC domains have been retained after fiber production (Figure 2b, **5 000**×). Such ordered fiber morphology is absent in the PU/MGO, PU/SGO and PU fibers because of the absence of fully nematic LC domains in their respective dispersions. It also shows that GO sheets are homogeneously

Table 1. GO sheet size characteristics of the three GO dispersions used in this study.

Sample	Mean [μm]	Maximum [μm]	Minimum [μm]	Median [μm]	Mode [μm]	Standard Deviation [μm]	Size Polydispersity (SPD)
LGO	12.2	38.8	1.1	10.3	6.0	8.2	0.67
MGO	2.5	15.7	0.2	1.8	0.4	2.4	0.96
SGO	0.3	1.2	0.1	0.3	0.1	0.2	0.57

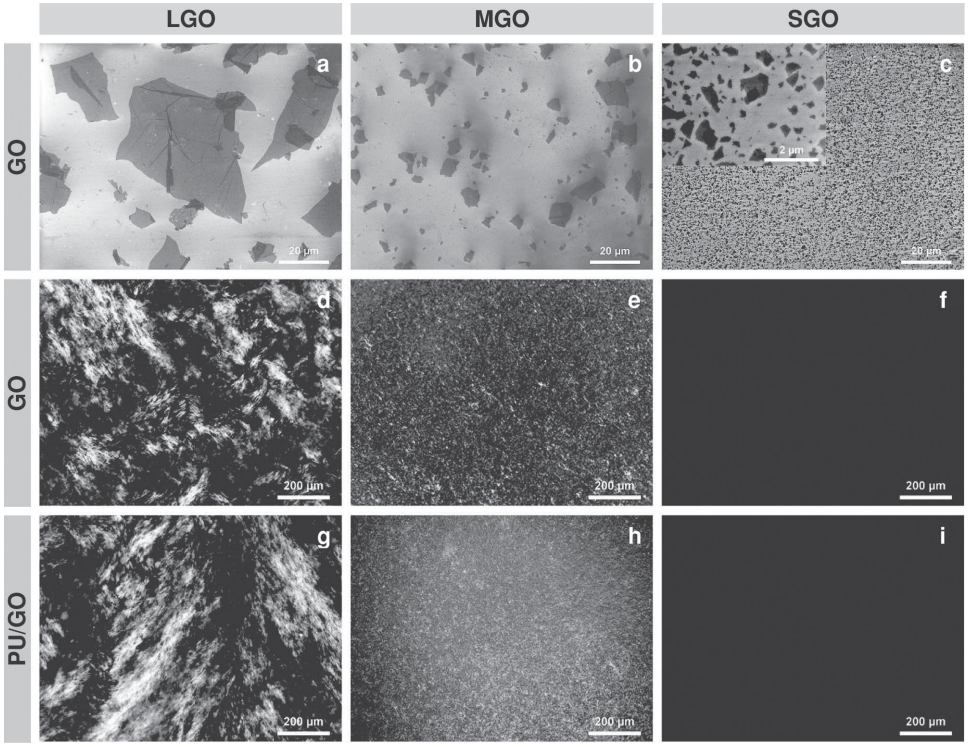

Figure 1. The sheet size dependent liquid crystalline behavior of pure graphene oxide (GO) dispersions is reflected in the polyurethane/graphene oxide dispersions. Representative SEM images of GO sheets in a) LGO, b) MGO and c) SGO dispersions. Also shown are representative polarized optical images of d) fully nematic LGO, e) biphasic MGO, and f) isotropic SGO dispersions at 1.5 mg ml^{-1} GO concentration. g–i) The respective PU/GO dispersions containing 1.5 mg ml^{-1} GO and 50 mg ml^{-1} PU show similar behaviors as the pure GO dispersions.

dispersed in the PU matrix and are predominantly aligned along the fiber axis (Figure 2b, **50 000**×).

2.2. Preferential Reinforcement Towards Hard Segment Domains

The uniaxial tensile stress-strain curves of the as-spun fibers in **Figure 3**a-b resemble those of typical thermoplastic elastomers.[16–19] The uniaxial tensile behavior of thermoplastic PU consists of three distinct regions (Figure S1a) i.e., an initial stiff response and yield (Region I, low strain range), strain-induced softening (Region II, plateau region), and finally, strain-induced hardening (Region III, crystallization region). Figure 3a-b clearly show significant improvements in low strain properties of PU fibers such as Young's modulus (*Y*) and yield stress (*YS*) upon the addition of GO sheets (highlighted in Region I) while retaining the high extensibility and strain hardening characteristics inherent to the PU soft segments (highlighted in Regions II and III). Notably, the observed reinforcements in *Y* and *YS* are sheet size dependent. The tensile extension-relaxation behavior confirmed the observed reinforcement in all PU/GO composite fibers with the extension cycles tracing the uniaxial tensile curves. **Figure 4**a shows such an example for PU/LGO fibers. Although there are significant differences between the loading and unloading paths during the extension-relaxation tests (suggesting hysteresis), all PU/GO fibers also showed very little change in permanent damage for applied strains of up to 400%. This result is depicted as the loss of elastic recovery (see Supporting Information for calculation) in respect to the pure PU fiber and shown in Figure 4c. Moreover, the 2.9 wt.% GO loading is significantly lower than the literature reports on filled elastomeric polymer composites, and the degree of reinforcement attained is much higher at the equivalent loading.[1–3]

It is apparent in Figure 3 that the low strain properties (Region I) are significantly enhanced much more effectively than the high strain properties (Regions II and III) suggesting preferential reinforcement in hard segments. Specifically in terms of *Y* (Figure 3c), the PU/LGO composite fibers exhibited a superior ~80-fold increase compared to the PU fiber, followed by the MGO (~60-fold) then SGO (~20-fold) fibers. A similar trend was observed for the improvement in *YS* (Figure 3d, stress at 5% strain) whereby the addition of LGO, MGO and SGO sheets resulted in a ~40-fold, ~25-fold and ~5-fold increase, respectively. It is also clear that the high strain properties remained unchanged suggesting that the mechanisms of extensions of PU soft segments are akin to the neat PU. All the three PU/GO fibers sustained high stresses after the initial yield and also exhibited high elongations of up to ~200% in region II before strain hardening became apparent in region III. In contrast to literature reports on reinforced elastomer composites that often have tensile strength and/or elongation at break of lower than their parent elastomer,[3,7,39] the PU/LGO and PU/MGO fibers have tensile strengths higher than PU (σ, Figure 3e). All PU/GO fibers retained high extensibilities greater than 400% (*E*, Figure 3f), resulting in higher toughness

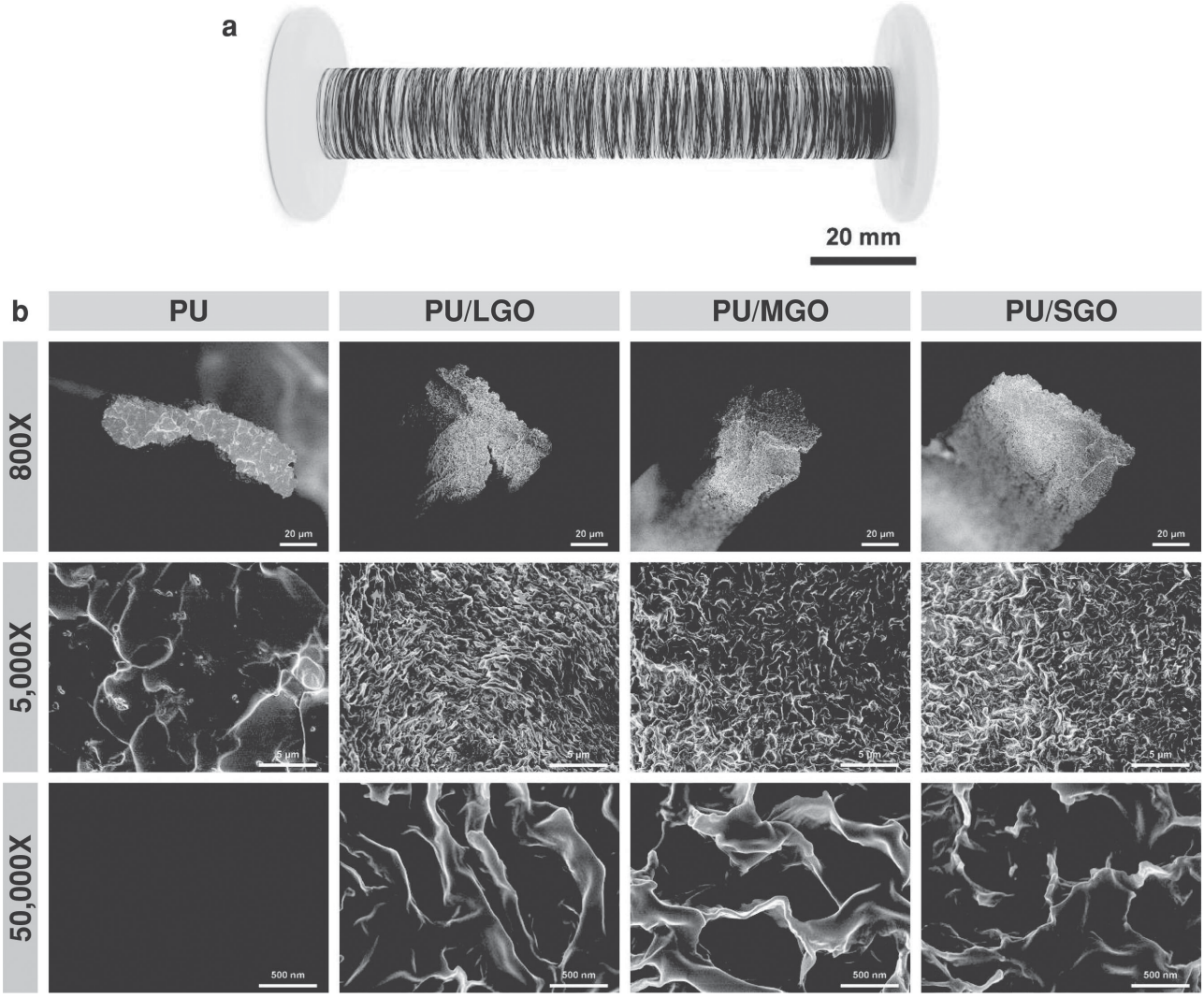

Figure 2. a) PU/GO fibers were continuously wet-spun and collected on a spool, b) the representative SEM images of fibers at increasing magnifications show that the differences in cross-sectional shape is influenced by the coagulation rate of each dispersion during fiber spinning (800×), the highly ordered domains in the nematic phase of the liquid crystalline PU/LGO dispersion is reflected in the morphology of the resulting fiber (5 000×); such ordering is absent in PU, PU/MGO and PU/SGO fibers, and the PU/GO domains, that are distinctly larger and thicker in PU/LGO fibers than other fibers, are aligned along the fiber axis (50 000×). All PU/GO fibers have 2.9 wt.% GO loading.

(*T,* Figure 3g) whereby approximately up to 3-fold increase in *T* was achieved in the PU/LGO and PU/MGO fibers.

The increase in *Y* and *YS* of the PU/GO fibers may be attributed to hydrodynamic effect[6,40–43] (also known as volume effect), which is the reinforcement achieved as a result of the addition of a significantly more rigid reinforcing filler (GO) to the relatively soft elastomeric host (PU). The high reinforcement in *Y* and *YS* of the PU/GO fibers also indicates strong interactions between the PU and GO, which are most likely facilitated by the presence of the functional groups in GO.[44] It is also clear that large sheet size magnifies the advantages of reinforcing polymers with GO. This latter observation is in agreement with the recent work by Khan et al., which has demonstrated that large solvent exfoliated graphene (SEG) sheets reinforce waterborne PU composites better than small SEG sheets.[3] The SEG sheets are however, ~40 times smaller than the LGO sheets used in this work, which could explain why very high loading of ~40 wt% SEG was necessary to achieve a comparable reinforcement in *Y* and *YS*. The use of large GO sheets have enabled *Y* and *YS* reinforcement at a very low GO loading of 2.9 wt% and had no deteriorating effect on *E*, in contrast to the ~10 times decrease in *E* on PU/SEG composites, and consequently, more than 20 times decrease in *T* due to the high SEG loading.

Given that PU comprises of hard segment domains (responsible for low strain properties such as *Y* and *YS*) and soft segment phase that can crystallize (for sustaining high σ at high ε), the very high *Y* and *YS* of the PU/LGO composite fiber in conjunction with the retained stretchability indicate that the hard segment domains are reinforced and the soft segment phase of PU is uninterrupted in the composite fiber. Both PU and PU/LGO fibers exhibited the same glass transition temperature of

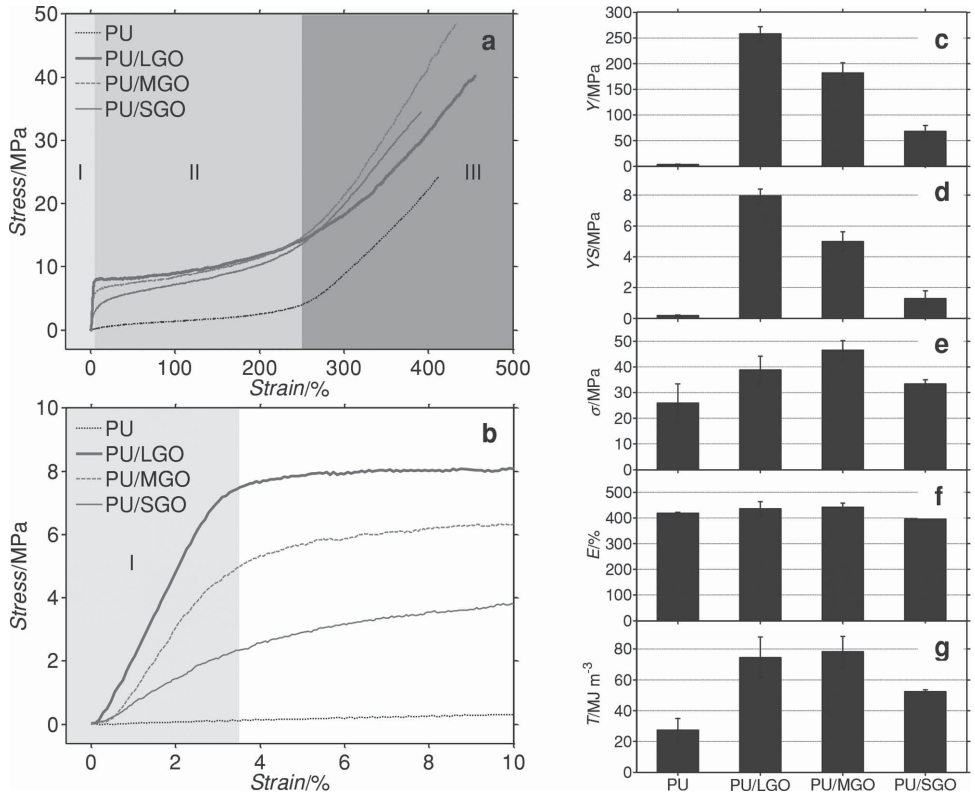

Figure 3. The representative stress-strain curves of PU and PU/GO fibers after a uniaxial tensile test showing a) the entire curve and b) magnification of region I to highlight the magnitude of differences in mechanical properties at the low strain region. The various mechanical properties derived from these curves, such as c) Young's modulus (*Y*), d) yield stress (*YS*, stress at 5% strain), e) tensile strength (σ), f) elongation at break (*E*), and g) toughness (*T*), highlight the significantly improved mechanical properties of as-spun PU/GO fibers in comparison to the neat PU fiber while retaining the elasticity inherent to PU.

~ –22 °C (Figure S2) confirming the uninterrupted soft segment phase in the composite fiber. This result in conjunction with the enhanced *Y* and *YS* also suggests that the GO sheets (and its LC phase, in the case of LGO and MGO samples) are highly compatible with the hard segment domains of PU (as depicted in **Scheme 1**). In contrast, since SGO sheets are isotropic, a global organization of PU/GO ordered domains is unlikely to be observed. This premise could also explain why the PU/LGO dispersions remained fully nematic and why the low strain properties of PU/LGO fibers are significantly higher than PU/SGO fibers, which is spun from an isotropic dispersion. Furthermore, the fiber spinning process further contributed to the flow-induced alignment of ordered PU/LGO domains as evidenced by the highly ordered microstructure within the PU/LGO fiber (Figure 2).

Reinforcement in soft segment phase, especially in region II, albeit minimal compared to reinforcement in hard segment domains cannot be ruled out. The higher stress at ε = 100% (σ_{100}) for all PU/GO fibers than for PU fibers (Figure S1b) confirms sustained reinforcement from GO towards the remaining unbroken small hard domains and soft segment chains. In fact, the higher modulus (Y_{II}) for all PU/GO fibers than for PU fiber in this region (Figure S1c) also suggests further alignment of small reinforced hard domains. In region III, however, the Y_{III} of all PU/GO fibers fall in the same range as that of PU (Figure S1d), suggesting that regardless of the addition of GO and irrespective of their sheet size, the sustained extensibilities of all PU/GO fibers even at high stresses allow for uninterrupted strain hardening in the PU soft segment phase.

Upon evaluating the stress softening behavior of the fibers with increasing applied strain, the preferential reinforcement of small hard segment domains upon extension (in region II) can also be observed. Stress softening, defined as the reduction in stress by strain history (as illustrated in Figure 4b), is typically attributed to the breakage and partial reconstruction of hard segment domains and formation of new cross-links between polymer chains.[18,42] It is apparent in Figure 4d that stress softening is significantly different between PU and PU/GO fibers only at applied strains below the strain hardening region (i.e., only in region II). This can be explained by the stiffening effect of GO at low strains, which enables the PU/GO fibers to attain and sustain higher stresses than the PU fiber. This higher stress is proportional to the amount of PU/GO domains and PU chains that are permanently broken, reflecting the large difference in stress softening for applied strains of up to 200%. Nevertheless, this difference becomes less significant when the magnitude of applied strain coincides with the strain hardening region (above 200% strain) where the stiffening effect of GO is less effective. For this region (region III), the similar level of stress softening between PU and PU/GO fibers suggest that stress softening originates mainly from the breakup of soft PU chains that have reached the limit of

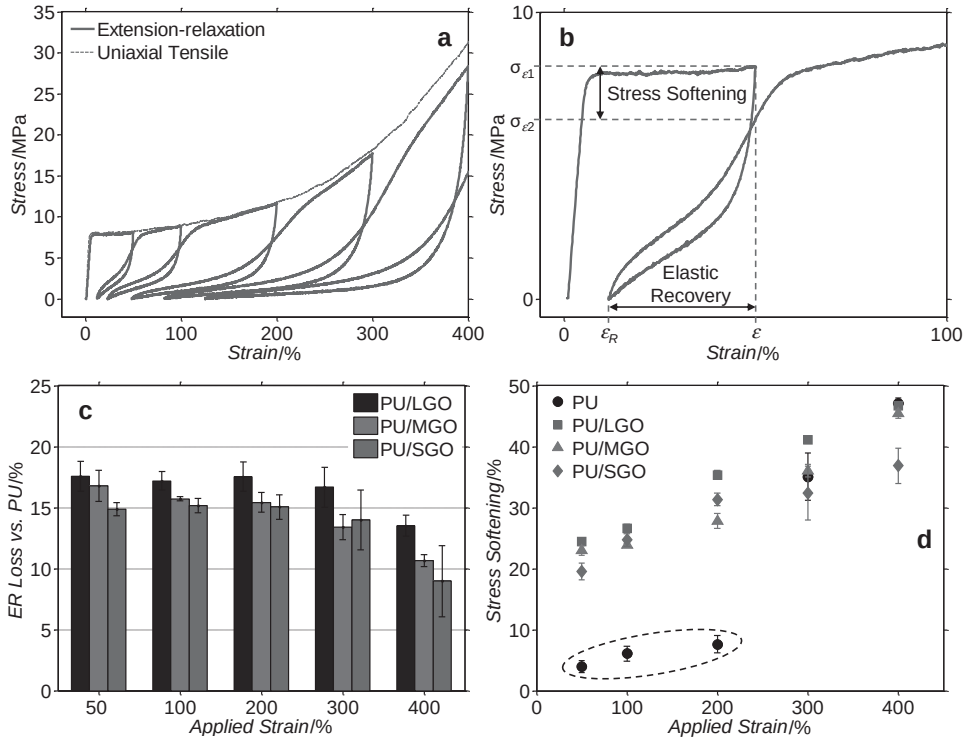

Figure 4. a) The representative stress-strain curve of PU/LGO fiber after the extension-relaxation tensile test. Also shown is an overlaid stress-strain curve of the same fiber after uniaxial testing. Shown in b) is a representation of where the relevant properties such as elastic recovery and stress softening are derived. From these data, c) The loss in elastic recovery (ER Loss) of PU/GO fibers with increasing applied strain relative to PU fiber and d) the stress softening of PU and PU/GO fibers with increasing applied strain were obtained using Equations S7 and S8 (Supporting Information), respectively.

their extensibility. These results further demonstrate that the use of GO does not disrupt the extension of soft PU chains to achieve high extensibilities.

2.3. Evaluation of Mechanical Performance Using Modulus and Elastic Recovery

Critical in realizing desirable properties of elastomeric composites for high performance applications is the ability to achieve a delicate balance between stiffness and elasticity while maintaining high extensibility.[2] In this regard, we evaluated the performance of the PU and PU/GO fibers by taking into account both modulus and elastic recovery in each extension-relaxation cycle reaching the applied strains of up to 400%. This was done by measuring moduli at the extension curves of each cycle (Y_ε) and the corresponding elastic recoveries after each extension-relaxation cycle (ER_ε). ER_ε values were taken as the normalized difference between applied strain and permanent set (*see* Supporting Information for calculation of ER_ε). As expected, the general behavior for all fibers show elastic recovery decreasing linearly (albeit slowly) with applied strain (**Figure 5**a) and modulus decreasing exponentially (Figure 5b). More importantly, the combined effect of modulus and elastic recovery represented as $Y_\varepsilon ER_\varepsilon$ (Figure 5c) clearly show the superior performance of PU/GO fibers over the neat PU fiber (higher $Y_\varepsilon ER_\varepsilon$) at all applied strains. Also apparent in these data is the sheet size dependence of $Y_\varepsilon ER_\varepsilon$.

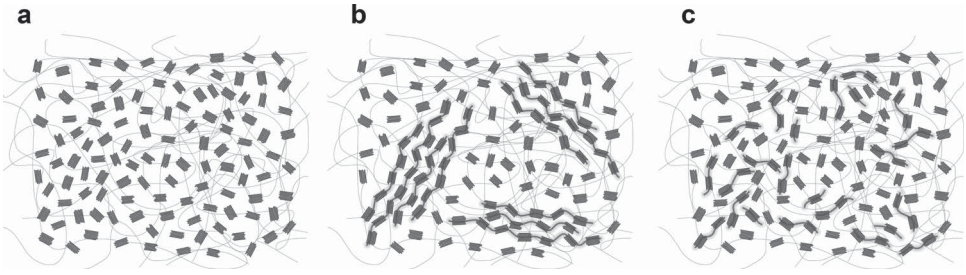

Scheme 1. a) Microstructural representation of PU consisted of random hard segment domains within the soft segment phase. b) Formation of highly ordered macro domains of PU hard segments organized on LC domains of LGO sheets. c) Such ordered hard segment macro domains are absent in PU/SGO. PU hard segment domain PU soft segment phase GO sheet.

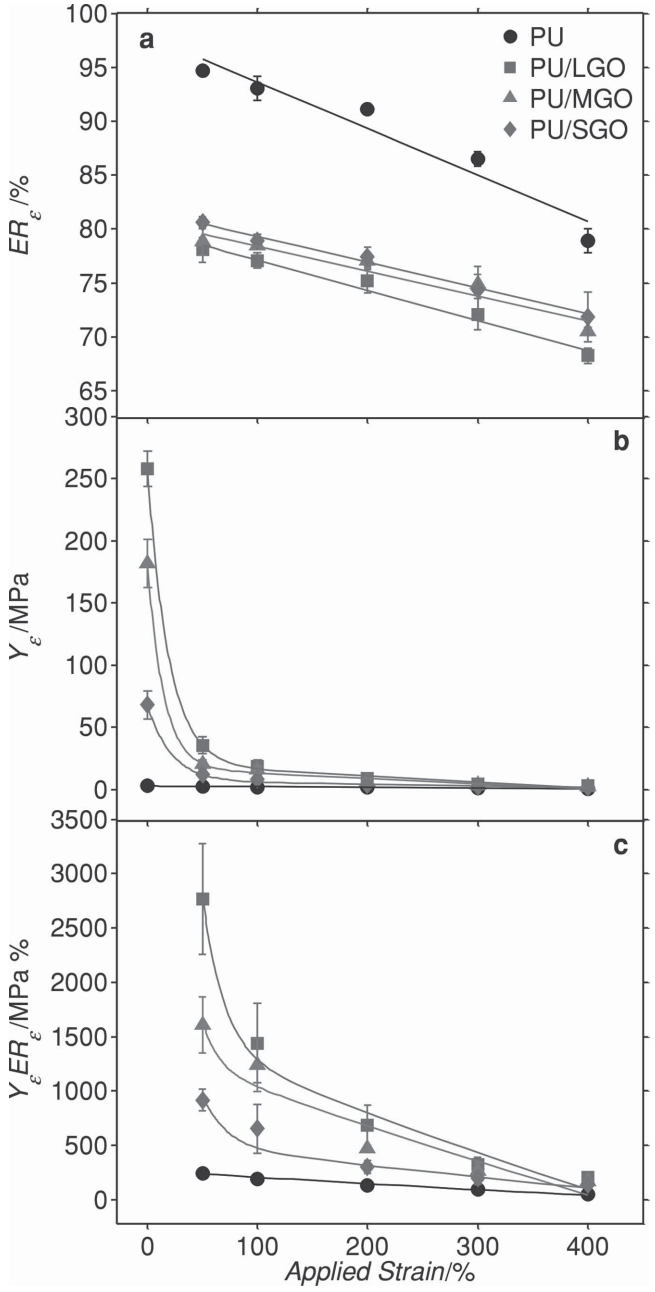

Figure 5. Comparison of the effect of GO sheet size on the a) elastic recovery, ER_ε, b) modulus, Y_ε, and c) $Y_\varepsilon ER_\varepsilon$ of the PU/GO composite fibers at different applied strains (ε = Applied Strain/100). The data fits are based on the proposed model in Equation (1).

The reduction in ER_ε with increasing applied strain represents the unrecoverable broken PU chains (and reinforced PU chains in the case of PU/GO fibers) in both the hard segment domain and soft segment phase.[19,45] The elastic recovery data suggests that more polymer chains in composite PU/GO fibers have been permanently damaged than in the neat PU fiber, understandably because the composite fibers are exposed to higher stresses at equivalent applied strains. The composite fibers are able to withstand high stress because reinforced hard segment domains are less vulnerable to rupture due to their higher stiffness. Even at high extensions, it can be observed that PU/GO fibers have Y_ε higher than PU suggesting effective reinforcement from GO even when PU chains have been damaged in the preceding extensions. This behavior further confirms that PU/GO fibers are able to exploit the reinforcing property of GO predominantly towards the hard segment domains (from the observed significant initial decrease in stiffness) without disrupting the high extensibility and elastic recovery property of the soft segment phase, as accentuated in the $Y_\varepsilon ER_\varepsilon$ plot. Furthermore, the observed sheet size dependent properties of PU/GO fibers demonstrate that the $Y_\varepsilon ER_\varepsilon$ performance can be modulated by varying the GO sheet size.

Because the nature of processing the GO dispersions to achieve GO sheets of various sizes also impact the sheet size distribution (i.e., dispersion in size), the maximum, mean and median sheet size attainable, and effectively, their LC behavior as in previous reports,[46,47] it is important to evaluate how each parameter will influence the mechanical properties of PU composites in order to exploit their true potential as reinforcing fillers. It is apparent that the highly ordered domains seen in PU/LGO (fully nematic) and PU/MGO (biphasic) formulations have been preserved in their respective fibers (Figure 2f). This maintained microstructural orders confirms the observed preferential reinforcement in the hard segment domains (over the soft segment phase), as evidenced by the enhanced low strain properties, uninterrupted strain-induced crystallization in the PU soft segment, and unchanged glass transition temperature of the PU. However, it is not clear how the GO sheet size dimension and dispersion of sheet size in the three formulations influence the observed trends.

To understand the origin of mechanical reinforcement in PU/GO fibers and which statistical sheet size values of GO sheets influence them and how, we fitted our data using a model in the form of Equation (1), which describes the observed mechanical behavior of the fibers with increasing applied strain (ε, in strain ratio). This equation accounts for the strain-dependent modulus behavior of the hard segment domains and soft segment phase of the fibers. A similar model has been used to describe the modulus behavior of PU/CNT composites.[8]

$$Y_\varepsilon = \left[T_H \cdot e^{-a\varepsilon}\right] + \left[Y_S - b\varepsilon\right] \quad (1)$$

According to Equation (1), the modulus of the fiber (Y_ε) at a given applied strain (ε) is estimated from the sum of the modulus of the hard segment domains (Y_H) that decreases exponentially by a factor of a, and the modulus of the soft segment chains (Y_S) that decreases linearly by a factor of b, Model parameters a and b correlate with how GO sheet size dimensions influence the rate of modulus decrease of both the hard segment domains and the soft segment phase, respectively. Note that Y_ε are obtained at the beginning of each extension cycle.

By fitting our data using Equation (1), it was found that the calculated values for Y_H are much greater than the Y_S for all fibers and are very close to the measured Y of all the fibers (**Table 2**). These data clearly indicate that the origin of high stiffness in PU/GO fibers arise predominantly from the reinforcement in hard segment domains than in the soft segment phase. It also follows that any damage when strain is applied is more likely to

Table 2. Experimental values for Young's modulus of the PU and PU/GO fibers and the derived values of the model parameters in Equation (1).

Sample	Y [MPa]	Y_H [MPa]	Y_S [MPa]	a	b [MPa]
PU	2.9 ± 0.8	2.8	0.15	0.34	0.05
PU/LGO	258 ± 14	238	20.0	5.2	4.7
PU/MGO	182 ± 20	165	17.2	6.8	4.1
PU/SGO	68 ± 11	61	6.7	4.7	1.3

occur in the PU hard segment domains because of the relatively higher extension of the PU chains in the soft segment phase. This observed preferential reinforcement towards hard segment domains have been previously reported using smectic clays[1] and carbon nanotubes.[2] However, to achieve the same level of reinforcement, filler loadings of more than 5 and 15 times than the current loading level were required, respectively. Note that the *Ys* of all PU/GO fibers are significantly higher than the Y_H of PU fibers indicating that even the reinforced soft segment phase of the PU/GO fibers are stiffer than the hard segment domains in pure PU.

In terms of reinforcement by GO sheet size, the Y_H of PU/GO fiber is ~85 times greater than that of PU, while it is only ~22 times higher for PU/SGO. Similar trend is observed for Y_S, which further confirms the superior reinforcement of large GO sheets in both hard and soft PU domains. We used the modulus efficiency factor (η_{LY}, which varies between 0 and 1)[48] defined in Equation (2), to evaluate at which conditions the modulus of the filler can be maximized, for this case, the dependence of the reinforcement on the GO sheet size.

$$\eta_{LY} = 1 - \frac{\tanh(nL/t)}{nL/t} \tag{2}$$

Where n is:

$$n = \sqrt{\frac{G_{PU}\phi}{Y_{GO}(1-\phi)}} \tag{3}$$

We used experimentally derived values in these equations to obtain the relationship between η_{LY} and the lateral GO sheet size (L) shown in **Figure 6**a, such that t is the thickness of the GO sheets (~1 nm), ϕ is the GO volume fraction (0.016), G_{PU} is the sheer modulus of PU (0.49 MPa) and Y_{GO} is the modulus of GO obtained from the Voigt model's rule of mixture.[49] We note that the experimentally derived Y_{GO} vary with sheet size (4.1, 11 and 16 GPa for SGO, MGO and LGO, respectively) and are much lower than the literature values of 200–500 GPa[50–53] (refer to Supporting Information for detailed calculations of these values). We also derived the η_{LY} vs L using Y_{GO} = 250 GPa in Figure 6a for comparison. When comparing different GO dispersions with various ranges of GO sheet sizes, it is critical to take into account the dispersity in size of the GO sheets as it is shown to influence Y_{GO} and η_{LY}. This is illustrated in Figure 6, which shows that the η_{LY} of a particular GO sheet in the SGO sample is higher than when the same sheet size is taken from the LGO sample. Furthermore, the maximum η_{LY} that can be achieved in a given range of GO sheet size is defined by the

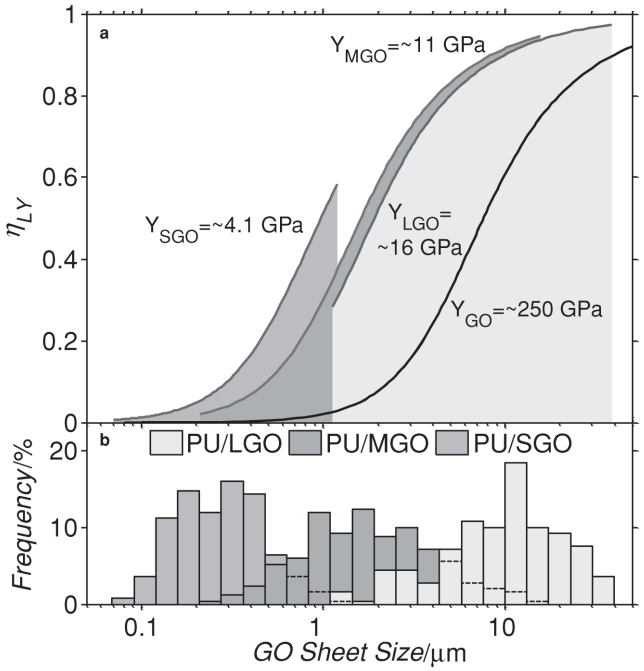

Figure 6. a) The relationship between the modulus efficiency factor (η_{LY}) and GO sheet size (L). b) The GO sheet size distribution for the respective LGO, MGO, and SGO dispersions are shown below the plot.

largest sheet size (e.g., 0.97 for LGO vs 0.58 for SGO). These results suggest that the size of other sheets in a given dispersion influence η_{LY}, i.e., the ability of a given sheet size to enhance the modulus of the composite is also dependent to the size of the other sheets in the sample. In order to account for the range of GO sheet sizes in a given sample, we calculated the normalized area under the curve (NA) for each dispersion using Equation (4).

$$\mathrm{NA} = \frac{1}{\mathrm{SPD}}\left(\int_{L_{min}}^{L_{max}} \eta_{LY}\, dL\right) \tag{4}$$

where L_{max} and L_{min} correspond to the maximum and minimum GO sheet size for each sample given in Table 1. NA is normalized with SPD to account for the difference in sheet size distribution in each GO sample. GO sheets of equal size (monodisperse) has been proven experimentally difficult to achieve to date, as illustrated by the dispersity in size even with as-synthesized GO that have not been exposed to any form of sonication (Table 1).

A linear correlation was found when NA was plotted against the various statistical values of sheet size in each GO sample, with mean GO sheet size (L_{mean}) being identified as the most linear and can therefore best represent the dependence of η_{LY} towards sheet size (Figure S3). It can also be observed that while η_{LY} increased very sharply with L, it was found to plateau at ~0.92 close to the L_{mean} of LGO (~12.2 μm). It can also be observed that it is only for LGO when η_{LY} plateaus at L_{mean}. Also, the L_{mean} of ~0.3 μm for SGO corresponded to η_{LY} ~0.11 that is strikingly lower than that of MGO (~0.66) and LGO (~0.92), both with higher L_{mean} of 2.5 μm and 12.2 μm, respectively. The low η_{LY} for this plot means that the maximum

attainable level of reinforcement is low, which is confirmed by our experimental data on PU/SGO fibers.

The η_{LY} at L_{mean} for SGO is strikingly low given that the Y_{GO} of 4.1 GPa is significantly lower than the literature value of 250 GPa, which if used, would correspond to a much lower η_{LY} (~0.002). Because η_{LY} increases quadratically with L, the corresponding η_{LY} values for MGO and LGO (when Y_{GO} = 250 GPa) are much higher than that of SGO given their significantly higher L_{mean}. These results further highlight the importance of maximizing GO sheet size for reinforcing PU. The data presented here suggests that L_{mean} > 10 μm is essential to maximize the reinforcement. This is in agreement with the previous observation on polyvinyl alcohol/SEG composites.[54]

We then correlated each model parameter in Equation (1) to η_{LY} to further evaluate the significance of L_{mean} and SPD in understanding the mechanisms of reinforcement in hard segment domain and soft segment phase of PU/GO fibers. It was found that the strain dependent moduli Y_H and Y_S, and the model parameter b were linearly correlated to η_{LY} at L_{mean} while the best linear fit for parameter a was observed with SPD (Figure S4). These correlations suggest that the modulus reinforcement in both hard segment domain and soft segment phase of PU/GO fibers is mainly influenced by sheet size. It also suggests that in the hard segment domains, the experimentally observed exponential decrease of Y_H with increasing applied strain (by a factor of a) can be attributed to the dispersity in size. Illustrated further, when two PU/GO composites with equal mean GO sheet size are compared (arguably these composites will have comparable Y_H based on above results), the composite that contains polydispersed sheets (i.e., one that contains a wide range of sheet size and/or one that contains more of small sheets than large sheets) is likely to have reinforced hard segment domains that fail at a much faster rate upon extension due to the low reinforcement from small sheets and the variation in sheet size distribution. In our experiments, the rapid drop in Y_H for PU/LGO fibers may be attributed to the presence of small sheets in LGO dispersions, which is consistent with the much lower Y_{GO} for small sheets (~4.1 GPa) than for large sheets (~16 GPa). In contrast, the observed linear decrease in Y_S (by a factor of b) is influenced by sheet size. In other words, enhancement of low strain properties (reinforcement of hard segment domains) would be most effective when GO sheet size is maximized and its size polydispersity minimized. Because the maximum enhancement in high strain properties (soft segment phase and small hard segment domains) is attained when GO sheet size is large, the proportional decrease in reinforcement during high extensions is also larger than when small sheets are used. These observed correlations clearly illustrate that the effect of GO reinforcement in the strain-dependent modulus behavior of PU/GO fibers in the soft segment phase (a function of GO sheet size) is significantly different than that in the hard segment domains (a function of both sheet size and size polydispersity). When a model was derived based on the correlations of the various parameters Y_H, Y_S, η_{LY} and b with L_{mean}, a, and SPD using the Equation (1), all models were found to agree very well to the fit of the strain dependent modulus experimental data (Figure S5) further confirming the validity of the derived interactions between various parameters used in modelling the PU/GO composites.

3. Conclusions

This study has shown that high mechanical performance of GO-based elastomeric fibers can be attained at a very low filler loading of only 2.9 wt.%, and in doing so, it is very important to consider the mean GO sheet sizes and the dispersion in their size distribution. It is also demonstrated that the cumulative effects of the liquid crystallinity of GO dispersions with mean sheet size greater than 10 μm is beneficial to the preferential reinforcement of the PU hard segment domains giving rise to significantly enhanced low strain properties such as Young's modulus and yield stress, without compromising high strain properties, like high extensibilities and only a marginal loss in elastic recovery. This superior mechanical performance achieved from a very simple method to produce liquid crystalline composite formulations that can be processed by a highly scalable wet-spinning approach will cater for a variety of applications and relevant industries in high-performance elastomeric fiber composites.

4. Experimental Section

Materials: Polycarbonate-based thermoplastic polyurethane (PU, AdvanSource Biomaterials Chronoflex C 80A), the elastomeric host in this study, was used as received. *N*,*N*-dimethylformamide (DMF) was purchased from Sigma-Aldrich and was used without further purification. Expandable graphite flakes (3772, Asbury Graphite Mills USA) were first thermally treated at 1050 °C for 15 sec and the resultant expanded graphite was used as precursor for synthesis of large graphene oxide (LGO).

Preparation of PU/GO Formulations: LGO Synthesis has been described elsewhere.[24,28] Stock LGO dispersion in DMF (1.5 mg ml^{-1}) was prepared by extraction of water from aqueous dispersion of LGO via repeated centrifugation and washing with DMF.[28] GO dispersions with medium GO (MGO) and small GO (SGO) sheet sizes were prepared from the stock LGO dispersion using bath sonication (Branson B1500R-MT, 50 W) for 10 min and probe sonication (Branson Digital Sonifier S-450D, 400 W, equipped with a 1/2" Disruptor Horn and a 1/8" Microtip) for 30 min at 30% amplitude, respectively. The respective PU/GO spinning formulations were prepared by dissolving PU pellets (for a PU final concentration of 50 mg ml^{-1}) into the GO dispersions in DMF (1.5 mg ml^{-1}).

Fiber Spinning: PU/GO fiber production was carried out according to the established wet-spinning technique in our lab.[24,34,35] The non-solvent of the coagulation bath was isopropanol, the spinning solution flow rate was kept at 5 ml h^{-1}, a 23 gauge needle was used as a spinneret, and the fibers were continuously collected onto a speed-controlled winder at 10 rpm.

Characterization: GO (LGO, MGO, and SGO) sheets were observed under SEM (JEOL JSM-7500FA) after depositing on silanized silicon wafer. Silicon substrates were immersed into a solution of 3-aminopropyltriethoxysilane (Aldrich) in water (1:9 v/v) with added a drop of hydrochloric acid (Sigma–Aldrich) for about 30 min and then rinsed with deionized water. GO sheets were deposited onto silanized silicon wafers by dipping in diluted GO dispersions (50 μg ml^{-1}) for about 5 seconds and air-drying the substrates. Lateral sheet sizes, i.e., diameter of equivalent circles, were then determined from at least 250 measurements from SEM images using ImageJ[55] image analysis software. GO and PU/GO dispersions in DMF were investigated for their birefringence under a polarizing optical microscope (POM, Leica DM EP) with 20X objective in bright field transmission-mode between crossed-polarizers. Samples were prepared by transferring approximately 200 μl of each dispersion onto a glass slide and confining the dispersion with a cover slip and sealing the edges. The morphology of the as-spun

PU/GO fibers was observed by a scanning electron microscopy (SEM) using a field emission SEM instrument (JEOL JSM-7500FA) after sputter coating (EDWARDS Auto 306) with platinum (~5 nm). Cross-section of PU/GO fibers was obtained by immersion of the fiber in liquid nitrogen for ~1 min and breaking the frozen fiber. An optical microscope (Leica DM EP) was used for measuring fibers diameters at 10 points along of the fiber. The mechanical properties of PU and PU/GO fibers were measured using a tensile testing instrument (Shimadzu EZ-L) with a 2 N load cell and 1 N grips for 10 samples per test. Samples were prepared by attaching the fibers onto paper frames (10 mm in aperture) and melting PU granules on top of the fiber using a soldering iron. This was necessary to avoid slippage during the mechanical tests due to better adherence achieved through usage of the same polymer. Sample was then mounted on the grips and secured and the paper was cut in the middle. For tensile test, fibers were stretched with strain rate (crosshead speed) of 10 mm min^{-1} (100% min^{-1}) until failure. Elastic recovery tests were also performed on PU and PU/GO fibers. In these tests, fibers were first stretched to 50% (strain rate of 10 mm min^{-1}) and then released to get back to their initial lengths (zero force). Fibers were further stretched to 100%, 200%, 300%, and 400% and released to zero stress each time. Elastic recovery at each strain was calculated using a coded program in MATLAB.

Supporting Information

Supporting Information is available from the Wiley Online Library or from the author.

Acknowledgements

This work is funded by the Australian Research Council (ARC) Centre of Excellence program and the University of Wollongong (UOW). JMR acknowledges funding from ARC Future Fellowship. The authors thank the Materials Node of Australian National Fabrication Facility (ANFF) and acknowledge use of the facilities and the assistance of Mr. Tony Romeo at the UOW Electron Microscopy Centre.

Received: July 1, 2014
Revised: August 26, 2014
Published online: October 13, 2014

[1] S. M. Liff, N. Kumar, G. H. McKinley, *Nat. Mater.* **2007**, *6*, 76.
[2] U. Khan, F. M. Blighe, J. N. Coleman, *J. Phys. Chem. C* **2010**, *114*, 11401.
[3] U. Khan, P. May, A. O'Neill, J. N. Coleman, *Carbon* **2010**, *48*, 4035.
[4] Z. Wang, T. J. Pinnavaia, *Chem. Mater.* **1998**, *10*, 3769.
[5] P. C. LeBaron, T. J. Pinnavaia, *Chem. Mater.* **2001**, *13*, 3760.
[6] H. Koerner, W. Liu, M. Alexander, P. Mirau, H. Dowty, R. A. Vaia, *Polymer* **2005**, *46*, 4405.
[7] F. M. Blighe, W. J. Blau, J. N. Coleman, *Nanotechnology* **2008**, *19*, 415709.
[8] U. Khan, P. May, A. O'Neill, J. J. Vilatela, A. H. Windle, J. N. Coleman, *Small* **2011**, *7*, 1579.
[9] B. Fernández-d'Arlas, U. Khan, L. Rueda, J. N. Coleman, I. Mondragon, M. A. Corcuera, A. Eceiza, *Compos. Sci. Technol.* **2011**, *71*, 1030.
[10] A. A. Gavrilov, A. V. Chertovich, P. G. Khalatur, A. R. Khokhlov, *Soft Matter* **2013**, *9*, 4067.
[11] D. A. Nguyen, Y. R. Lee, A. V Raghu, H. M. Jeong, C. M. Shin, B. K. Kim, *Polym. Int.* **2009**, *58*, 412.
[12] A. V. Raghu, Y. R. Lee, H. M. Jeong, C. M. Shin, *Macromol. Chem. Phys.* **2008**, *209*, 2487.
[13] Y. R. Lee, A. V. Raghu, H. M. Jeong, B. K. Kim, *Macromol. Chem. Phys.* **2009**, *210*, 1247.
[14] H. Kim, Y. Miura, C. W. Macosko, *Chem. Mater.* **2010**, *22*, 3441.
[15] N. Yousefi, M. M. Gudarzi, Q. Zheng, X. Lin, X. Shen, J. Jia, F. Sharif, J.-K. Kim, *Compos. Part A Appl. Sci. Manuf.* **2013**, *49*, 42.
[16] M. Szycher, *Szycher's Handbook of Polyurethanes*; 2nd Ed.; CRC Press: Boca Raton, **2013**.
[17] Z. S. Petrović, J. Ferguson, *Prog. Polym. Sci.* **1991**, *16*, 695.
[18] F. Yeh, B. S. Hsiao, B. B. Sauer, S. Michel, H. W. Siesler, *Macromolecules* **2003**, *36*, 1940.
[19] E. M. Christenson, J. M. Anderson, A. Hiltner, E. Baer, *Polymer* **2005**, *46*, 11744.
[20] J. W. Dieter, C. A. Byrne, *Polym. Eng. Sci.* **1987**, *27*, 673.
[21] D. K. Chattopadhyay, K. V. S. N. Raju, *Prog. Polym. Sci.* **2007**, *32*, 352.
[22] Z. Xu, C. Gao, *Nat. Commun.* **2011**, *2*, 571.
[23] Z. Dong, C. Jiang, H. Cheng, Y. Zhao, G. Shi, L. Jiang, L. Qu, *Adv. Mater.* **2012**, *24*, 1856.
[24] R. Jalili, S. H. Aboutalebi, D. Esrafilzadeh, R. L. Shepherd, J. Chen, S. Aminorroaya-Yamini, K. Konstantinov, A. I. Minett, J. M. Razal, G. G. Wallace, *Adv. Funct. Mater.* **2013**, *23*, 5345.
[25] Z. Xu, H. Sun, X. Zhao, C. Gao, *Adv. Mater.* **2013**, *25*, 188.
[26] C. Xiang, C. C. Young, X. Wang, Z. Yan, C.-C. Hwang, G. Cerioti, J. Lin, J. Kono, M. Pasquali, J. M. Tour, *Adv. Mater.* **2013**, *25*, 4592.
[27] Z. Xu, C. Gao, *Acc. Chem. Res.* **2014**, *47*, 1267.
[28] R. Jalili, S. H. Aboutalebi, D. Esrafilzadeh, K. Konstantinov, S. E. Moulton, J. M. Razal, G. G. Wallace, *ACS Nano* **2013**, *7*, 3981.
[29] Z. Liu, Z. Xu, X. Hu, C. Gao, *Macromolecules* **2013**, *46*, 6931.
[30] X. Zhao, Z. Xu, B. Zheng, C. Gao, *Sci. Rep.* **2013**, *3*, 3164.
[31] A. J. Granero, P. Wagner, K. Wagner, J. M. Razal, G. G. Wallace, M. in het Panhuis, *Adv. Funct. Mater.* **2011**, *21*, 955.
[32] R. Jalili, J. M. Razal, P. C. Innis, G. G. Wallace, *Adv. Funct. Mater.* **2011**, *21*, 3363.
[33] R. Jalili, J. M. Razal, G. G. Wallace, *J. Mater. Chem.* **2012**, *22*, 25174.
[34] R. Jalili, J. M. Razal, G. G. Wallace, *Sci. Rep.* **2013**, *3*, 3438.
[35] M. Z. Seyedin, J. M. Razal, P. C. Innis, G. G. Wallace, *Adv. Funct. Mater.* **2014**, *24*, 2957.
[36] A. Ziabicki, *Fundamentals of Fibre Formation: The Science of Fibre Spinning and Drawing*; Wiley: London, **1976**.
[37] C. Liu, J. Cuculo, B. Smith, *J. Polym. Sci. Part B Polym. Phys.* **1990**, *28*, 449.
[38] S. P. Mishra, *A Textbook of Fibre Science and Technology*; New Age International: New Delhi, **2000**.
[39] Y. C. Jung, J. H. Kim, T. Hayashi, Y. A. Kim, M. Endo, M. Terrones, M. S. Dresselhaus, *Macromol. Rapid Commun.* **2012**, *33*, 628.
[40] A. Voet, *J. Polym. Sci. Macromol. Rev.* **1980**, *15*, 327.
[41] G. Huber, *Macromolecules* **2002**, *35*, 9204.
[42] L. Bokobza, *Macromol. Mater. Eng.* **2004**, *289*, 607.
[43] T. A. Vilgis, G. Heinrich, M. Klüppel, in *Reinforcement of Polymer Nano-Composites*; Cambridge University Press: Cambridge, **2009**; pp. 101–117.
[44] D. R. Dreyer, S. Park, C. W. Bielawski, R. S. Ruoff, *Chem. Soc. Rev.* **2010**, *39*, 228.
[45] D. Puett, *J. Polym. Sci. Part A-2 Polym. Phys.* **1967**, *5*, 839.
[46] J. E. Kim, T. H. Han, S. H. Lee, J. Y. Kim, C. W. Ahn, J. M. Yun, S. O. Kim, *Angew. Chem. Int. Ed. Engl.* **2011**, *50*, 3043.
[47] R. Jalili, S. H. Aboutalebi, D. Esrafilzadeh, K. Konstantinov, J. M. Razal, S. E. Moulton, G. G. Wallace, *Mater. Horizons* **2014**, *1*, 87.
[48] G. E. Padawer, N. Beecher, *Polym. Eng. Sci.* **1970**, *10*, 185.
[49] W. Voigt, *Wied. Ann.* **1889**, *38*, 573.

[50] J. T. Paci, T. Belytschko, G. C. Schatz, *J. Phys. Chem. C* **2007**, *111*, 18099.
[51] C. Gómez-Navarro, M. Burghard, K. Kern, *Nano Lett.* **2008**, *8*, 2045.
[52] J. W. Suk, R. D. Piner, J. An, R. S. Ruoff, *ACS Nano* **2010**, *4*, 6557.
[53] A. Zandiatashbar, G.-H. Lee, S. J. An, S. Lee, N. Mathew, M. Terrones, T. Hayashi, C. R. Picu, J. Hone, N. Koratkar, *Nat. Commun.* **2014**, *5*, 3186.
[54] P. May, U. Khan, A. O'Neill, J. N. Coleman, *J. Mater. Chem.* **2012**, *22*, 1278.
[55] Image J. *http://rsb.info.nih.gov/ij/* (accessed September 2014).